Progressive Failure Modeling of Tailored Universal Feedstock for Forming (TuFF) Discontinuous Long Fiber Composites

Brett A. Bednarcyk[1], Evan J. Pineda[1], Javier Buenrostro[2], Joshua Stuckner[1], Anthony A. Mosto[3], Jamal F. Husseini[3], Scott E. Stapleton[3], and Sandi G. Miller[1]

[1] NASA Glenn Research Center, Cleveland OH 44135, USA
[2] University Space Research Association (USRA), Cleveland OH 44135
[3] University of Massachusetts Lowell, Lowell MA 01854, USA

Abstract. Progressive failure modeling, via the NASA Multiscale Analysis Tool (NASMAT), has been performed for a novel discontinuous composite system. The composite, known as Tailored Universal Feedstock for Forming (TuFF), retains properties comparable to continuous fiber composites, but, due to its discontinuous fibers, it is much more formable. Based on serial sectioning image data, a two-dimensional micromechanics model of TuFF has been developed. This representation sufficiently captures the key features of the microstructure yet remains quite computationally efficient. Through the use of an energy-based crack band damage model for the matrix, it is demonstrated that accurate predictions of the TuFF damage and failure can be made. Further, the effect of the matrix toughness, which is a key input to the crack band model, is examined.

Keywords: TuFF, Modeling, Damage, Failure, Toughness, PEKK, Microstructure.

1 Introduction

Discontinuous fiber composites are typically reinforced with particles or relatively short fibers. This maximizes formability and minimizes cost, but due to low fiber volume fractions, fiber misalignment, and the large percentage of the fiber length that is ineffective, the properties of short fiber discontinuous composites are not competitive with continuous fiber composites. Stretch broken continuous fibers improve formability while retaining continuous composite properties, but with their fiber length to diameter aspect ratio on the order of 7000, they are still significantly less formable than typical discontinuous composites [1]. A novel composite system, developed by the University of Delaware – Center for Composite Materials, utilizing a fiber length to diameter ratio of approximately 600, has demonstrated sheet metal-like processing capabilities while also retaining properties similar to continuous fiber composites [1, 2]. This new composite system is named Tailored Universal Feedstock for Forming (TuFF). The material's highly aligned discontinuous long fibers provide stiffness and strength comparable to continuous fiber composites, but with vastly improved

formability. This enables production of complex shaped parts with significant cost reductions compared to continuous fiber composites. Like all composites, TuFF's characteristics arise from its constituent materials and unique microstructure. As such, micromechanics is ideal for modeling TuFF's microstructure and its impact on the overall macroscopic mechanical behavior [3].

Herein micromechanics models for TuFF composites have been developed using the NASA Multiscale Analysis Tool (NASMAT) [4, 5] informed by serial sectioning image data. These image data have been segmented using Otsu's method [6] in conjunction with cleaning operations. The NASMAT model is shown to capture the relevant nonlinear mechanisms including fiber stiffening, fiber end debonding, and matrix shear splitting. Comparison is made between the NASMAT model predictions and tensile test data for the composite elastic properties and progressive failure/strength.

2 TuFF Composite Material

Tailored Universal Feedstock for Forming (TuFF) is an advanced discontinuous carbon fiber composite developed at the University of Delaware's Center for Composite Materials (UD-CCM) [1, 2]. It features highly aligned discontinuous long fibers embedded in a thermoplastic matrix, enabling manufacturing techniques typically associated with metal, such as forming, and the integration of recycled constituents, offering cost advantages over conventional continuous fiber composites [1]. When the fiber alignment is maintained within ±5° (around 95% alignment), and fiber aspect ratios (length-to-diameter) exceed 600, TuFF materials can reach fiber volume fractions as high as 63%. Under these conditions, their stiffness and strength properties closely match those of continuous fiber counterparts [7]. However, the mechanical behavior of these composites remains sensitive to the microstructure [8].

The present study considers TuFF composites composed of IM7 carbon fibers and a polyetherketoneketone (PEKK) thermoplastic matrix. Composite panels were manufactured at the University of Delaware, while neat PEKK panels were manufactured at NASA Glenn Research Center. Specimens were machined at Cincinnati Testing Laboratories, and mechanical tests were performed on the composite at the University of Arizona and on the neat PEKK at Ohio State University [9]. The neat PEKK test data were used as input for the micromechanics analyses, whereas the model predictions were compared to the longitudinal tensile test results for the TuFF composite.

To evaluate the TuFF composite microstructure, serial sectioning was performed using a Robo-Met system, which automatically sections, polishes, and images a sample at high resolution [10]. When combined, the sections provide three-dimensional data on the composite microstructure. For the TuFF composite, 100 serial sectioning images were obtained, with dimensions 1292 × 968 pixels, with an example shown in Fig. 1. Note that misaligned fibers appear more ovular, and they are clearly associated with a matrix rich band as aligned fibers pass over and under the misaligned fiber.

As described in detail in ref. [11], Otsu's method [6] was used to segment the serial sectioning images into fiber and matrix regions. Statistics on the fiber spacing, fiber diameter, fiber alignment, and location/proximity of fiber ends were then determined.

It was found that the composite had an overall fiber alignment score of 0.989 (on a scale from 0 to 1), indicating very high fiber alignment [11], with the vast majority of fibers having a misalignment of less than 5°. This informed the micromechanics model, leading to the decision to treat the fibers as perfectly aligned in the model.

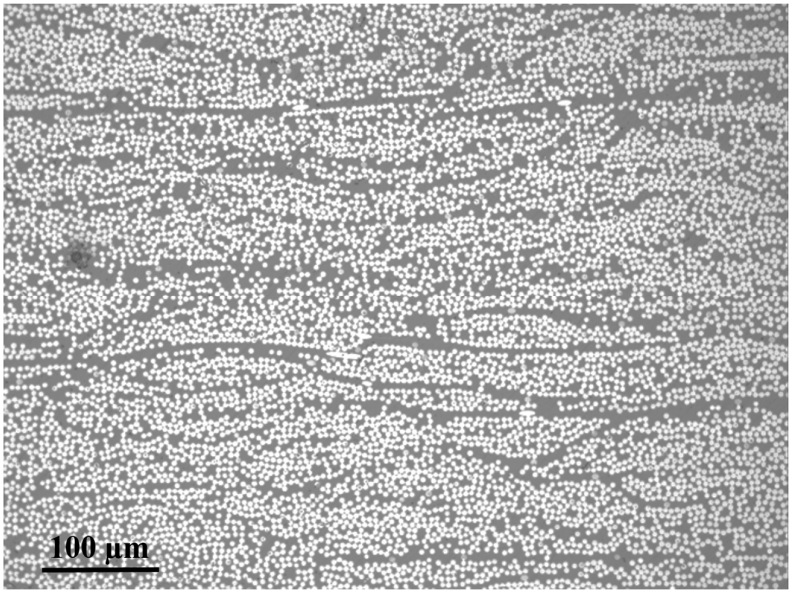

Fig. 1. Example image from the serial sectioning of the IM7/PEKK TuFF composite.

The fiber end detection results were also quite informative for the micromechanics model. In a volume of 0.084 mm^3, 971 fiber ends were detected, with a mean distance between nearest neighbor fiber ends of 32.1 µm. The histogram of these data, along with an image of one cross-section (inset) are shown in Fig. 2. The red markings in the image indicate the three fiber ends that were associated with this particular (nearest) cross-section. Note that the nearest neighbor fiber end for each of these three could be out of this plane. Based on these data, indicating that the mean nearest neighbor fiber end is approximately 6.5 fiber diameters, it was determined that fiber end mechanical interaction is quite unlikely and almost certainly not a primary driver of the TuFF composite's mechanical behavior. Even relatively close fiber ends are likely bridged by multiple fibers. As such, when constructing the micromechanics model, care was taken to ensure minimal mechanical interaction between fiber ends.

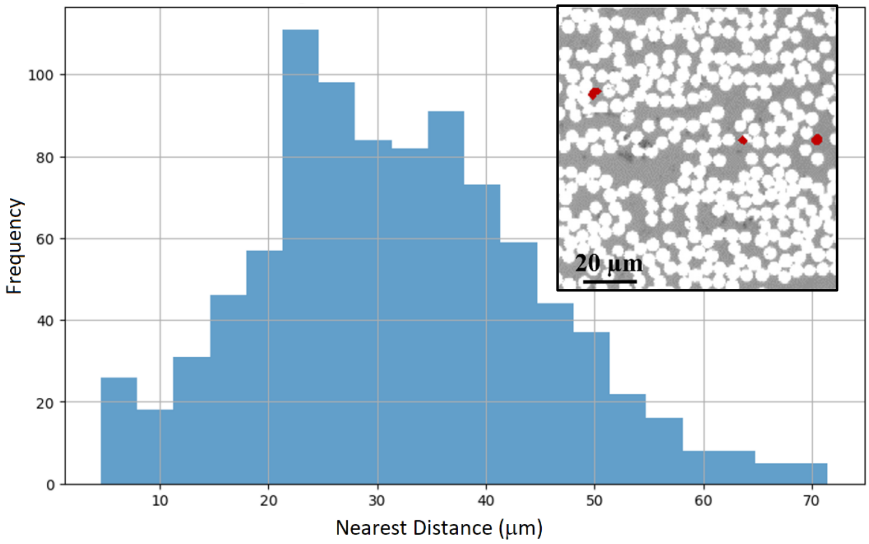

Fig. 2. Histogram of nearest neighbor distances for the detected fiber ends within a serially sectioned TuFF sample. Inset: image of one section with nearby detected fiber ends indicated in red.

3 Micromechanics Model

3.1 High-Fidelity Generalized Method of Cells (HFGMC) Repeating Unit Cell (RUC)

The well-documented High-Fidelity Generalized Method of Cells (HFGMC) micromechanics theory [12, 13] was used to predict the longitudinal tensile response of the IM7/PEKK TuFF composites. Summarizing, this semi-analytical approach analyzes a repeating unit cell composed of rectangular parallelepiped subvolumes. Assuming a quadratic displacement field in each subvolume, equilibrium is enforced within each subvolume and continuity between subvolumes, as well as periodicity, are enforced via the surface averaged tractions and displacements. This results in a system of linear algebraic equations that can be solved to obtain the effective (homogenized) properties of the RUC, as well as the local fields in each subvolume. Both doubly-periodic (considering a 2-D RUC) and triply-periodic (considering a 3-D RUC) formulations of the HFGMC theory are available [12, 13]. The HFGMC theory has been implemented in the NASA Multiscale Analysis Tool (NASMAT) [4, 5], which includes nonlinear effects such as progressive damage and plasticity.

To focus on the primary drivers of the TuFF composite response, a doubly-periodic HFGMC RUC in the plane transverse to the fiber direction has been considered. This enables capture of the fiber ends, the correct length of the fibers, and the damage

mechanisms involving the fiber ends and matrix splitting along the fibers. A similar triply-periodic RUC could have also been employed, but each simulation would be considerably more computationally demanding. Both the number of fibers in the RUC and the subvolume discretization were studied closely, and it was determined that a baseline RUC of 4 fibers with a relatively coarse discretization gave very similar predictions compared to more refined RUC and RUCs including more fibers. Considering fewer than 4 fibers affected the predicted failure mechanisms, whereas, RUCs with up to 50 fibers were evaluated and showed no benefit over the 4 fiber baseline. Likewise, two levels of higher subvolume discretization density were considered, also offering no discernable benefit over the coarsest baseline discretization.

The baseline 4 fiber RUC, shown in Fig. 3 was employed for the predictions in this study. This is a reasonably simple representation, but, as will be shown, it captures the primary mechanisms affecting the TuFF composite progressive damage response. Each of the 4 fibers is perfectly aligned, 3 mm long, and 5 μm in diameter (matching the nominal TuFF dimensions). The fiber ends are simply modeled as a gap in the fiber, but it is important that this gap is long enough such that the local stress fields at the fiber ends do not interfere with each other (as indicated by the microstructure data discussed in Section 2). A gap length of 50 μm has been employed, and it was confirmed by examining and plotting the local stresses at and around the fiber ends that this ensures that the local fields around each fiber end are independent. The subvolume discretization is biased such that it is denser in the vicinity of the fiber ends. There are only 2 subvolumes between subcells, but as mentioned, doubling and quadrupling this refinement had almost no effect on the model predictions. The RUC discretization is 12 × 426 subvolumes, and the fiber spacing was chosen to result in the desired fiber volume fraction of 0.55 (matching the experimental average).

Fig. 3. HFGMC RUC used to simulate the IM7/PEKK TuFF composite. (a) Fibers are black, matrix is gray, with no discretization shown. (b) Discretization shown. (c) Detail showing the discretization near fiber ends.

3.2 Crack Band Matrix Damage/Failure Model

The crack band model, originally proposed in ref. [14], has been modified and implemented within NASMAT to model failure in the PEKK matrix material. This continuum damage theory assumes that the fracture energy due to cracking in the material is dissipated over the entire volume of the continuum subvolume containing the damaging

zone, or crack band. The relationship between the traction on, and separation of, the crack faces within the crack band are governed by a traction versus separation law, and the area under the traction-separation law is equal to the fracture toughness of the material, which is a model input. In the NASMAT implementation, it is assumed that the crack band aligns normal to one of the basis vectors in the local material coordinate frame, and the cracks evolve under a mixed-mode (power-law) relationship (see ref. [15] for details).

3.3 IM7 Carbon Fiber Stiffening

The longitudinal tensile tests on the IM7/PEKK TuFF composites, as well as similar tests on unidirectional IM7/PEKK, exhibited noticeable stiffening [9]. Oliveira et al. [16] observed and quantified the elastic stiffening behavior of IM7 carbon fibers. Ruland [17] proposed a mechanism for this behavior based on unwrinkling of the connections between graphitic layers in carbon fibers. Oliveira et al. [16] quantified the IM7 fiber stiffening based on,

$$\varepsilon_{11} = \frac{\sigma_{11}}{E_{11}} + \delta\left(\frac{\sigma_{11}}{E_{11}}\right)^2 \tag{1}$$

where E_{11} is the initial longitudinal Young's modulus, σ_{11} and ε_{11} are the longitudinal stress and strain, respectively, and δ is an empirical constant. The (inverse of the) apparent Young's modulus can then be determined as,

$$\frac{1}{\bar{E}_{11}} = \frac{\varepsilon_{11}}{\sigma_{11}} = \frac{1}{E_{11}} + \delta\frac{\sigma_{11}}{E_{11}^2} \tag{2}$$

Oliveira et al. [16] determined the following values of E_{11} and δ for the IM7 fiber,

$$E_{11} = 264.1 \pm 16.0 \text{ GPa}, \qquad \delta = -4.96 \pm 0.23 \tag{3}$$

Fig. 4 shows the longitudinal nonlinear elastic stress-strain response of the fiber, according to the work of Oliveira et al. [16] compared with the linear elastic response of the IM7 fiber according to the vendor-supplied Young's modulus of 276 GPa [18]. The slight difference in initial Young's modulus (264.1 vs. 276 GPa) is barely noticeable, but at a longitudinal strain of 0.025, Eq. (2) indicates a (secant) Young's modulus of 309 GPa (11% stiffer compared to the vendor Young's modulus).

Fig. 5 shows the effect of including the fiber stiffening on the longitudinal tensile response of a 0.58 fiber volume fraction unidirectional IM7/PEKK composite, along with experimental data [9]. Clearly, including the fiber stiffening in the model significantly improves the predicted composite deformation response with respect to the correlation with the experimental data.

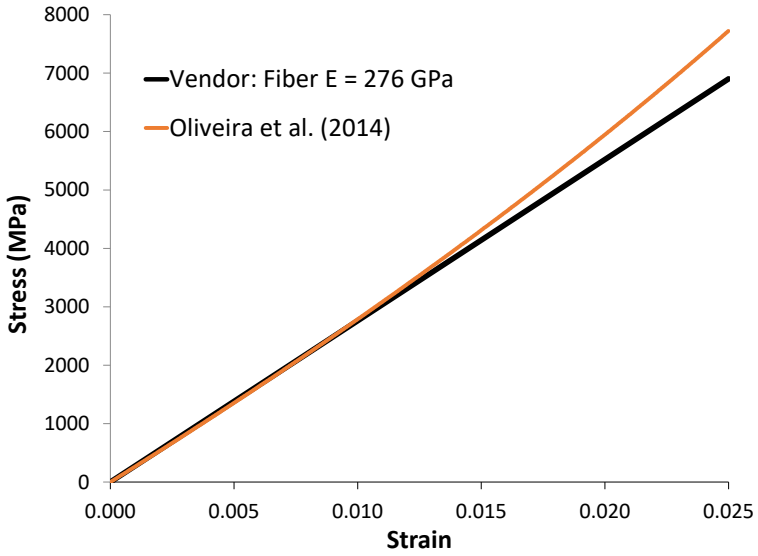

Fig. 4. Comparison of the stress-strain response of an IM7 carbon fiber treated as linearly elastic with the vendor-supplied Young's modulus vs. the fiber stiffening equation (2) of Oliviera et al. [16].

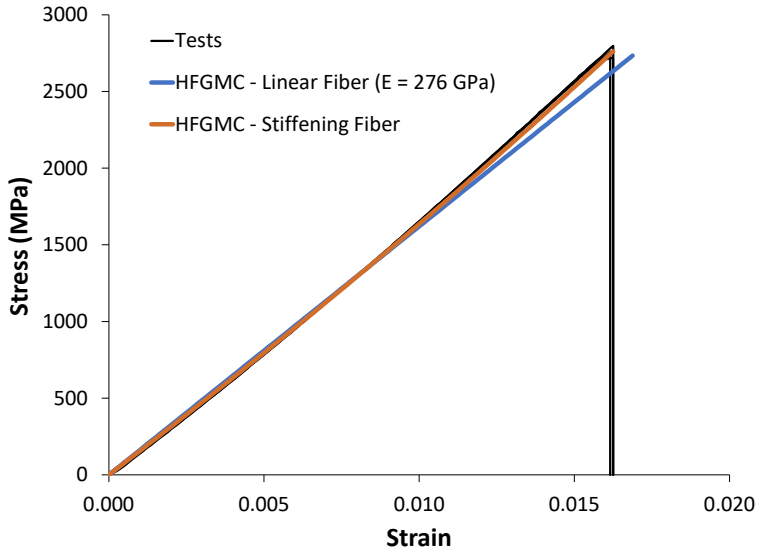

Fig. 5. Micromechanics predictions of the longitudinal stress-strain response of a 0.58 fiber volume fraction continuous IM7/PEKK composite.

3.4 Constituent Material Properties

The PEKK matrix was treated as isotropic, with elastic properties obtained from tests on neat PEKK specimens [9]. The IM7 fiber was treated as transversely isotropic and elastic, with a longitudinal Young's modulus that stiffened under longitudinal loading according to Eq. (2). These properties are given in Table 1.

The failure of the IM7 fiber was dictated by the maximum strain criterion, which was only active in the longitudinal direction. A nominal failure strain of 2% was employed. The progressive damage and failure of the PEKK matrix was dictated by the crack band model (see Section 3.2). The mode I and mode II damage initiation tractions were taken as the average tensile and shear strengths (respectively) from the neat PEKK tests [9]. Fracture toughness tests for the PEKK matrix were not conducted, and reliable toughness data (for the neat matrix, as opposed to interlaminar composite data) were not available. Through discussions with Arkema [19], the supplier of the PEKK thermoplastic, a value for the mode I fracture toughness, G_{IC}, of 11 N/mm was obtained. Because this value is not well-known nor documented, and it is quite high, sensitivity studies were performed with the model regarding the mode I fracture toughness, with this value as a baseline. To obtain a reasonable value for the mode II fracture toughness, G_{IIC}, the mode I value was scaled based on the mode II to mode I interlaminar fracture toughness data for a carbon/PEKK composite provided by Toray [20]. This ratio G_{IIC}/G_{IC} of 1.44 was maintained for all simulations when varying the PEKK toughness. These damage and failure parameters are listed in Table 2.

Table 1. Constituent elastic properties.

	E_{11} (GPa)	E_{22} (GPa)	ν_{12}	ν_{23}	G_{12} (GPa)
PEKK Matrix	4.454	4.454	0.4212	0.4212	1.567
IM7 Fiber	264.1*	14	0.25	0.25	20.

* This is the IM7 initial modulus, used in Eq. (2) with δ = -4.96, to capture fiber stiffening.

Table 2. Constituent damage/failure properties.

	Mode I damage initiation traction (MPa)	Mode II damage initiation traction (MPa)	Baseline G_{IC} (N/mm)	Baseline G_{IIC} (N/mm)	Mixed-mode power law exponent
PEKK Matrix	118.7	71.9	11	15.8*	1
IM7 Fiber	Brittle, longitudinal failure strain = 0.02				

* Based on 1.44 ratio with G_{IC}.

4 Results and Discussion

4.1 Simulated Damage Mechanisms

Fig. 6 illustrates the typical damage progression in the IM7/PEKK TuFF composite during simulated longitudinal tensile loading. One of the four regions including fiber ends is highlighted. Damage initiates at the fiber ends (consistent with Ref. [21]). The damage then transitions to shear splitting between the fibers along the length of the RUC.

Fig. 7 shows the longitudinal strain in the IM7 fibers, in a region of fiber ends, immediately before and after breakage of a fiber is predicted. Before the fiber breaks, the adjacent fibers bridging the fiber ends are overloaded compared to fibers further from the fiber ends. This then results in a fiber subvolume in this region exceeding its strain to failure in the simulation (i.e., a simulated fiber break).

Fig. 8 illustrates that the fiber shear splits can run the length of the composite and link up, causing final failure of the composite. This can occur without fiber breaks (for instance, if the fiber strain to failure was very high), or in conjunction with fiber breaks (as shown in Fig. 8). As will be shown, this predicted final failure behavior is dependent on the fracture toughness of the PEKK matrix.

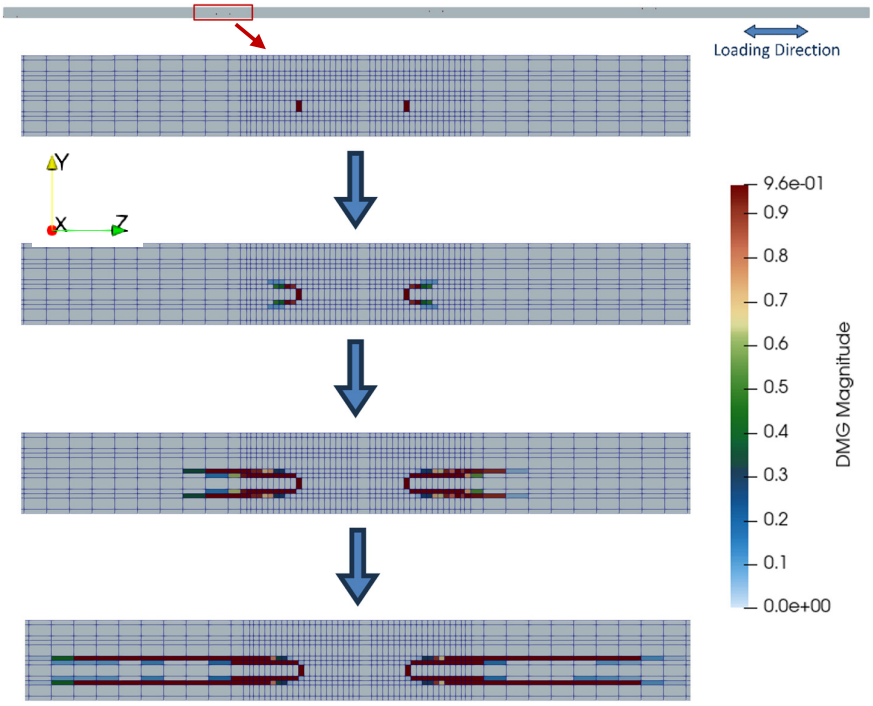

Fig. 6. Progressive damage evolution in a IM7/PEKK TuFF composite during simulated longitudinal tensile loading.

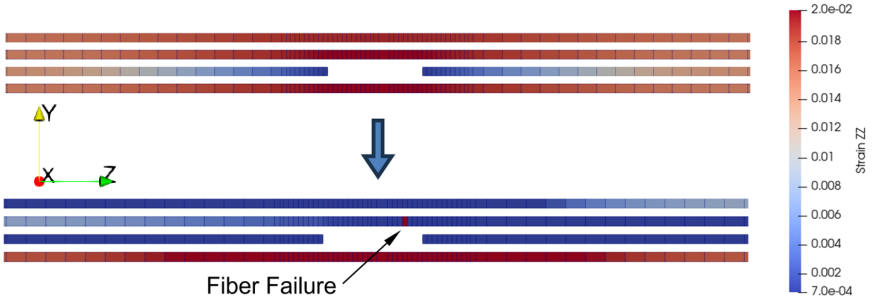

Fig. 7. Longitudinal strain in the fibers immediately before and after a fiber break in a region including fiber ends.

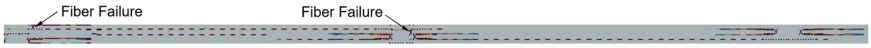

Fig. 8. The fiber shear splitting can run and link up, causing simulated final failure of the composite. This can occur before, or in conjunction with, fiber breakage.

4.2 Correlation with Experimental Data

Fig. 9 compares the HFGMC model predictions for the TuFF composite with experimental data [9]. Model prediction with and without fiber stiffening are shown. Clearly, the inclusion of fiber stiffening has significantly improved the correlation with the test data, particularly at the higher strain levels. The arrows in Fig. 9 indicate the onset of damage at the fiber ends and the onset of splitting damage. This is quite early in the simulation, and there is no obvious sign in the global response indicating that damage has initiated. The progression of the fiber splitting is slow, and the predicted strength of the TuFF composite is 2.8 times the damage initiation stress.

The final failure prediction in Fig. 9 appears good, but this is dependent on the fiber strain to failure, which was simply taken as 0.02. A more rigorous fiber failure model would account for the statistical nature and length scale effects to enable consistent predictions for both the TuFF composite and its unidirectional counterpart (see Fig. 5).

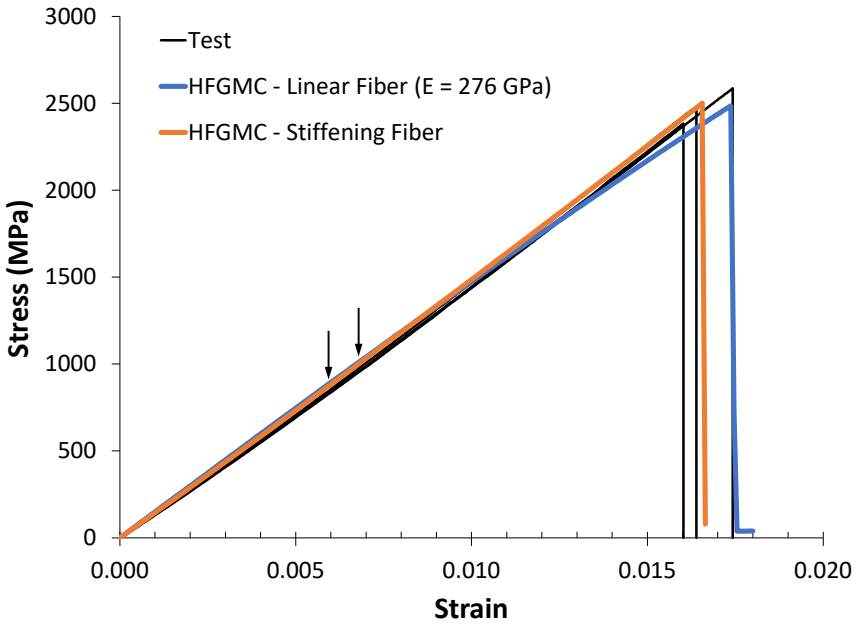

Fig. 9. Comparison of the HFGMC model predictions for the longitudinal tensile response of a 0.55 fiber volume fraction IM7/PEKK TuFF composite with test data [9]. Predictions with both linear elastic and stiffening IM7 fibers are shown. The arrows indicate the initiation of damage at the fiber ends and initiation of shear splitting.

4.3 Sensitivity of Predictions to PEKK Matrix Toughness

To examine the sensitivity of the HFGMC predictions to the PEKK matrix fracture toughness (which, recall, is not well-known), simulations were conducted with the PEKK G_{IC} and G_{IIC} values successively divided by 2. The ratio of G_{IIC} to G_{IC} was maintained at 1.44. This treats the matrix as successively more and more brittle. Results are shown in Fig. 10.

Interestingly, for the five simulations with the tougher matrix (G_{IC} = 0.688 N/mm and above), the toughness value has almost no effect on the prediction. This is because, when the matrix is sufficiently tough, the fiber breakage initiates before the shear splits between the fibers run. The onset of fiber breakage is associated with the large drop in stress in the stress-strain response, indicated simulated final failure. In contrast, if the matrix is sufficiently brittle, the splits run before the initiation of fiber breakage. This also causes a large drop in the stress, indicating predicted final failure. It is clear from Fig. 10 that this transition in the final failure mechanism occurs between G_{IC} values of 0.688 N/mm and 0.344 N/mm (corresponding to G_{IIC} values of 0.99 N/mm and 0.5 N/mm).

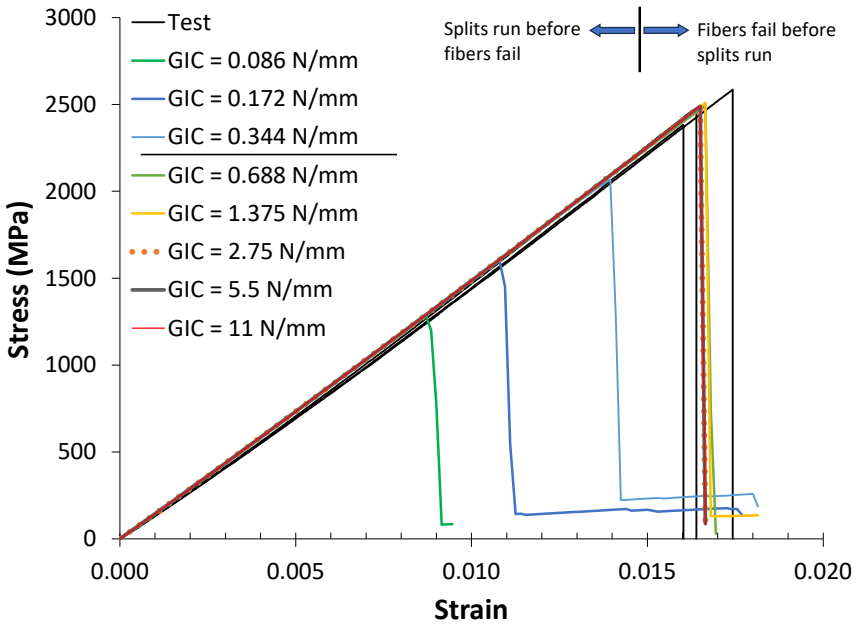

Fig. 10. Sensitivity of the TuFF composite longitudinal tensile response to the PEKK matrix mode I fracture toughness, G_{IC}, value. Note that, in all case, G_{IIC} is taken as 1.44 times G_{IC}.

Fig. 11 shows the final damage/final failure patterns for the toughest and most brittle cases from the Fig. 10 sensitivity study. With the very tough PEKK matrix, the matrix shear splitting between fibers progresses quite far, but the fiber breakage occurs before the splitting runs. For the brittle matrix case, there is some fiber breakage present, but this has occurred after the matrix splits have run and widely linked up.

These results indicate the necessity of employing a tough matrix (like PEKK) in TuFF composites. If the matrix is too brittle, the matrix splits will run (causing composite final failure) before the fibers break. To take full advantage of the high strength of the fibers, the matrix must be sufficiently tough so as to prevent the splits from running until after the initiation of fiber breakage.

A post-test photo of an IM7/PEKK TuFF longitudinal tensile specimen is shown in Fig. 12 [9]. There is clear evidence of fiber breakage and matrix splitting but, obviously, there is no way to determine the order of these events.

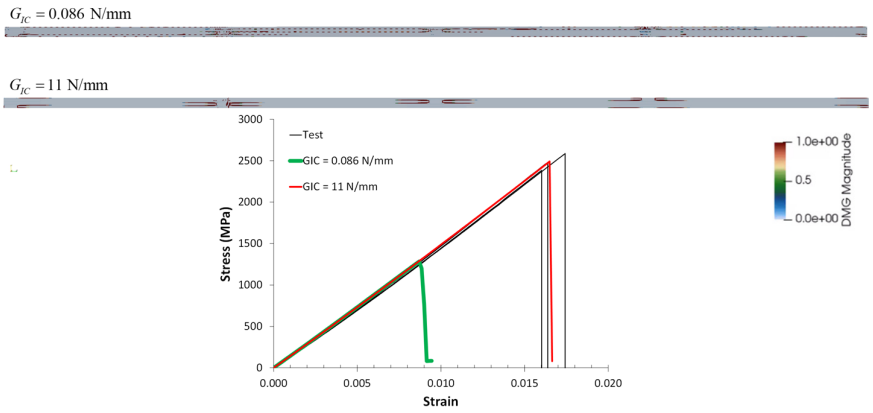

Fig. 11. Comparison of the final damage pattern between the toughest and most brittle cases from Fig. 10. The global stress-strain curves are shown for reference.

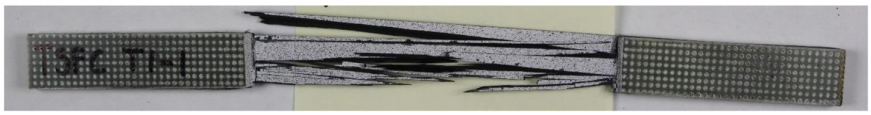

Fig. 12. Post-test photo of one of the TuFF longitudinal tensile specimens [9].

5 Conclusion

A progressive failure modeling framework has been developed and applied to the novel Tailored Universal Feedstock for Forming (TuFF) discontinuous long fiber composite using the NASA Multiscale Analysis Tool (NASMAT). The model integrates high-fidelity micromechanics via the High-Fidelity Generalized Method of Cells (HFGMC), a matrix crack band damage formulation, and nonlinear fiber stiffening behavior to accurately simulate the progressive damage and failure mechanisms of the IM7/PEKK TuFF system. Crucially, microstructural input to the model was informed by segmented serial sectioning image data. This allowed for a realistic representation of fiber geometry, spacing, and end distributions, leading to highly efficient yet representative micromechanics simulations. The model predictions exhibited excellent correlation with experimental stress-strain behavior, particularly when fiber stiffening was included, and captured critical features such as the onset and progression of fiber-end damage and matrix shear splitting.

Sensitivity analyses demonstrated that the fracture toughness of the PEKK matrix plays a pivotal role in determining the ultimate failure mode of the TuFF composite. When the matrix is sufficiently tough, failure is governed by fiber breakage, allowing the composite to fully exploit the high strength of the carbon fibers. In contrast, a brittle

matrix promotes premature matrix splitting, limiting overall composite strength. These findings highlight the importance of carefully selecting or tailoring matrix properties in TuFF composites to ensure optimal performance. Overall, this work confirms that with proper micromechanical modeling and material design, long discontinuous fiber composite systems like TuFF can deliver structural performance comparable to continuous fiber composites while offering the manufacturing flexibility and cost advantages of sheet-formable materials.

References

1. Yarlagadda, S., Deitzel, J., Heider, D., Tierney, J., Gillespie, J.W.: Tailorable universal feedstock for forming (tuff): overview and performance. SAMPE 2019, Charlotte, NC, May (2019).
2. Cender, T.A., Simacek, P., Gillespie, J.W., Advani, S.: Microstructural evolution of highly aligned discontinuous fiber composites during longitudinal extension forming, Composites Science and Technology 254, 110649, DOI: 10.1016/j.compscitech.2024.110649 (2024).
3. Kaleel, I., Pineda, E.J., Bednarcyk, B.A.: Micromechanical modeling of discontinuous long fiber reinforced composites. Mechanics of Advanced Materials and Structures. DOI:10.1080/15376494. 2024.2352798 (2024).
4. Pineda, E.J., Bednarcyk, B.A., Ricks, T.M., Arnold, S.M., Henson, G.: Efficient multiscale recursive micromechanics of composites for engineering applications. International Journal for Multiscale Computational Engineering 19(4). DOI: 10.1615/IntJMultCompEng. 2021039732 (2021).
5. National Aeronautics and Space Administration, NASA Multiscale Analysis Tool (NASMAT) version 4.0, https://software.nasa.gov/software/LEW-20650-1 (2025).
6. Otsu, N.: A threshold selection method from gray-level histograms. IEEE Transactions on Systems, Man, and Cybernetics, 9(1), 62–66. https://doi.org/10.1109/ TSMC.1979.4310076 (1979).
7. Yarlagadda, S., Advani, S., Deitzel, J., Heider, D., Molligan, D., Roseman, D., Simacek, P., Tierney, J., Gillespie, J.: Formability of tuff composite blanks. SAMPE 2019, Charlotte, NC, May (2019).
8. Heider, D., Tierney, J., Henchir, M., Gargitter, V.: Microstructural evaluation of aligned, short fiber tuff material, SAMPE 2019, Charlotte, NC, May (2019).
9. Maurya, A., Pechetti, S., Chen, H., Rajan, S., Buenrostro, J., Pereira, J.M., Miller, S.G.: Experimental Tests to Characterize the Behavior and Properties of HexPly Continuous Fiber Unidirectional Composite & TuFF Discontinuous Fiber Composite, NASA/TM-20250004308 (2025).
10. BlueHalo, https://bluehalo.com/emerging-technology/materials-and-processes/ (2025).
11. Mosto, A.A., Stuckner, J., Pineda, E.J., Bednarcyk, B.A., Husseini, J.F., Stapleton, S.E.: Microstructure characterization of highly aligned discontinuous fiber composites. in preparation (2025).
12. Aboudi, J., Arnold, S.M., Bednarcyk, B.A.: Micromechanics of Composite Materials A Generalized Multiscale Analysis Approach, Elsevier, Oxford, UK (2013).
13. Aboudi, J., Arnold, S.M., Bednarcyk, B.A.: Practical Micromechanics of Composite Materials, Elsevier, Oxford, UK (2021).

14. Bažant, Z.P., Oh, B.H.: Crack band theory for fracture of concrete, Matériaux et Construction 16, 155-177 (1983).
15. Ricks, T.M., Pineda, E.J., Bednarcyk, B.A., McCorkle, L.S., Miller, S.G., Murthy, P.L.N., and Segal, K.N.: Multiscale progressive failure analysis of 3D woven composites" Polymers, 14(20), 4340, DOI: 10.3390/polym14204340 (2022).
16. Oliveira, L., Hichcock, D., Behlow, H., Podila, R., Skove, M.J., Serkiz, S.M., Roa, A.M.: Second and third-order elastic constants of filaments of HexTow IM7 carbon fiber. Journal of Materials Engineering and Performance 23, pp. 685-692, DOI: 10.1007/s11665-013-0826-2 (2014).
17. Ruland, W.: The relationship between preferred orientation and Young's modulus of carbon fibers. Applied Polymer Symposia 9, pp. 293–301 (1969).
18. Hexcel: HexTow IM7 carbon fiber datasheet. https://www.hexcel.com/user_area/content_media/raw/IM7_HexTow_DataSheet.pdf (2023).
19. Arkema, Personal Communication, 27 February (2025).
20. Toray, Toray Cetex® TC1320 PEKK Product Data Sheet, https://www.toraytac.com/media/409dcc72-6aff-4643-86b8-20b5f464f038/lNO6TA/TAC/Documents/Data_sheets/Thermoplastic/UD%20tapes,%20prepregs%20and%20laminates/Toray-Cetex-TC1320_PEKK_PDS.pdf (2025).
21. Chen, B.R., Prakash, K., Yarlagadda, S., Gillespie, J.W.: Fatigue performance of thermoplastic TuFF composites, SAMPE 2022, Charlotte, NC, May (2022).